GENETICS

Targeting therapeutic vulnerabilities with PARP inhibition and radiation in IDH-mutant gliomas and cholangiocarcinomas

Yuxiang Wang[1], Aaron T. Wild[2,3], Sevin Turcan[4], Wei H. Wu[1], Carlie Sigel[5], David S. Klimstra[5], Xiaoxiao Ma[1], Yongxing Gong[1], Eric C. Holland[6], Jason T. Huse[7], Timothy A. Chan[1,2,8]*

Mutations in isocitrate dehydrogenase (IDH) genes occur in multiple cancer types, lead to global changes in the epigenome, and drive tumorigenesis. Yet, effective strategies targeting solid tumors harboring IDH mutations remain elusive. Here, we demonstrate that IDH-mutant gliomas and cholangiocarcinomas display elevated DNA damage. Using multiple in vitro and preclinical animal models of glioma and cholangiocarcinoma, we developed treatment strategies that use a synthetic lethality approach targeting the reduced DNA damage repair conferred by mutant IDH using poly(adenosine 5′-diphosphate) ribose polymerase inhibitors (PARPis). The therapeutic effects are markedly enhanced by cotreatment with concurrent, localized radiation therapy. PARPi-buttressed multimodality therapies may represent a readily applicable approach that is selective for IDH-mutant tumor cells and has potential to improve outcomes in multiple cancers.

INTRODUCTION

Neomorphic mutations in the genes encoding isocitrate dehydrogenase 1 and 2 (*IDH1/2*) have been identified in multiple cancer types, including lower grade glioma (LGG) (*1*), secondary glioblastoma (*2*), intrahepatic cholangiocarcinoma (ICC) (*3*, *4*), acute myeloid leukemia (AML) (*5*), chondrosarcoma (CS) (*6*), and others. The mutant IDH enzyme (IDHmut) converts the Krebs cycle intermediate α-ketoglutarate (αKG) into 2-hydroxyglutarate (2-HG), which functions as an oncometabolite. 2-HG can induce global DNA hypermethylation, inhibition of histone lysine demethylases, and block of cell differentiation (*7*–*10*). One strategy to treat IDHmut tumors is to inhibit the mutant IDH protein and 2-HG production. This is being tested in IDH-mutated cancers. Recently, inhibitors of IDH2 (enasidenib) and IDH1 (ivosidenib) have been shown to induce differentiation of cancer cells in patients with recurrent or refractory AML (*11*, *12*). However, this approach has been much less effective for solid tumors in both clinical and experimental contexts. Paradoxically, exogenous 2-HG can cause toxicity and slow down cell proliferation by inhibiting mammalian target of rapamycin signaling and mRNA m6A modification (*13*, *14*). Furthermore, 2-HG directly inhibits homologous recombination (HR), thus weakening DNA damage repair (DDR) and potentially improving the outcome from DNA damaging agents in patients receiving standard-of-care cytotoxic therapies (*15*, *16*). *IDH* mutations are associated with better outcomes from radiation therapy (RT) and chemotherapy in patients with glioma. It has been hypothesized that therapeutic modalities that inhibit 2-HG production in gliomas may abolish such protection and promote unfavorable evolution of the disease. Our previous work demonstrated that IDHmut causes genetic instability linked to accelerated copy number alterations throughout the genome (*10*). Biochemical studies showed that 2-HG inhibits HR-dependent repair and confers poly(adenosine 5′-diphosphate) ribose polymerase inhibitor (PARPi) sensitivity (*16*–*19*). However, the therapeutic potential for this phenomenon remains ill-defined. Moreover, it remains to be seen whether this approach is sufficient by itself or needs to be combined with other therapeutic modalities.

PARP1 (and other PARPs) play critical roles in the repair of DNA single-strand breaks (SSBs) through base excision repair, nucleotide excision repair, and other DNA damage response pathways (*20*). PARP inhibition leads to persistence of unrepaired SSBs and cytotoxic PARP-DNA complexes, which, when encountered at the replication fork, leads to the formation of potentially lethal DNA double-strand breaks (DSBs) (*21*). Cells with deficient HR, the main compensatory mechanism to manage the increased DSB stress imposed by PARPi, are unable to efficiently repair these DSB and enter mitotic catastrophe and apoptosis (*22*). We hypothesized that the HR deficiency induced by 2-HG across different solid tumors would fit this model of synthetic lethality, leading to marked sensitivity to PARPi in IDHmut tumors. Moreover, ionizing radiation (IR), alone or in combination with surgical resection, is routinely used in the clinic as a part of standard of care in treating cancers including LGG and ICC. By rapidly introducing high numbers of exogenous DNA SSB and DSB, IR exacerbates the effects of deficiency of DDR in HR-deficient tumors. Early trials combining IR with PARPi have shown promise in the BRCA-mutant context (*23*). However, PARPis as radiosensitizers for other types of HR-deficient tumors have not been thoroughly tested in preclinical or clinical settings. In this study, we showed that IDHmut tumor samples from patients with LGG and ICC harbor markedly elevated levels of DNA damage. We demonstrate in multiple in vitro contexts that expression of mutant IDH1 sensitizes the cell to radiation and PARPi. Last, we used two orthotopic LGG and one heterotopic ICC xenograft animal model to show that PARPi sensitizes the tumors to IR and that this sensitization

[1]Human Oncology and Pathogenesis Program, Memorial Sloan Kettering Cancer Center, New York, NY 10065, USA. [2]Department of Radiation Oncology, Memorial Sloan Kettering Cancer Center, New York, NY 10065, USA. [3]Southeast Radiation Oncology, Charlotte, NC 28204, USA. [4]Max-Eder Junior Group on Lower Grade Gliomas, Heidelberg University Hospital, Heidelberg, Germany. [5]Department of Pathology, Memorial Sloan Kettering Cancer Center, New York, NY 10065, USA. [6]Human Biology Division, Fred Hutchinson Cancer Research Center, Seattle, Washington, DC 98109, USA. [7]Departments of Pathology and Translational Molecular Pathology, University of Texas MD Anderson Cancer Center, Houston, TX 77030, USA. [8]Immunogenomics and Precision Oncology Platform (IPOP), Memorial Sloan Kettering Cancer Center, New York, NY 10065, USA.
*Corresponding author. Email: chant@mskcc.org

is specifically associated with *IDH* mutation status. Overall, our study demonstrates that IR markedly augments the therapeutic effects of PARPi and provides evidence supporting the combinatorial use of PARPi with IR to treat IDH-mutant tumors.

RESULTS

Therapeutic vulnerability conferred by mutant IDH1 to PARPi and IR in vitro

Previous studies have suggested that repair of DNA damage by HR is impaired by mutant IDH1 expression in a human colon cancer cell line through the oncometabolite 2-HG (*16*). To ascertain whether this effect is generalizable, we first used an immortalized human astrocyte (IHA) isogenic cell line system, which includes one line that expresses mutant IDH1 R132H (IHA-IDH1mut), and a matching isogenic control, which does not express mutant IDH1 (IHA-EV) (*10*). Expression of mutant IDH1 induces changes in the DNA methylation and histone landscape, which recapitulates those in IDH1-mutant tumors and blocks differentiation (*7*, *10*). We first subjected IHA-EV and IHA-IDH1mut to staining of γ-H2AX histones. As shown, IHA-EV demonstrates low levels of γ-H2AX–positive foci, whereas IHA-IDH1mut exhibits elevated levels of γ-H2AX staining (Fig. 1A and fig. S1A). These cells were fixed at the exponentially proliferative stage without being exposed to exogenous DNA damaging agents. The DSBs marked by γ-H2AX positivity in IDH1mut cells indicates a higher level of unrepaired DNA damage. To further support this finding, we performed Western blots to examine the level of phospho–KRAB-associated protein 1 (KAP1), an enzyme downstream of ATM (ataxia telangiectasia mutated). IHA-IDH1mut displayed notably higher levels of KAP1 phosphorylation compared to IHA-EV, suggesting increased engagement of the replication stress pathway (Fig. 1, B and C). However, consistent with previous reports (*10*, *14*, *16*), these unrepaired DNA damage sites did not induce significant change in cell death, likely due to concurrent inactivation of p53 as a part of immortalization. IDH-dependent defects in DDR may function as a driving force to produce additional mutations in the founder population during malignant progression. Next, we hypothesized that this rescue by p53 inactivation can be overcome by excessive DNA damage that accumulates in IDH1mut cells beyond a critical threshold. As observed in BRCA-mutant malignancies, the defective DSB repair in HR-defective tumors is often compensated for by other DDR pathways such as nonhomologous end joining, which, in turn, may themselves contribute to disease progression by inaccurate repair. We reasoned that the IDH1mut-induced DDR deficiency can be targeted by PARP inhibition similar to the scenario in BRCA-mutant breast and ovarian cancer and that this synthetic lethality could be augmented by inflicting further DNA damage through radiotherapy.

To test our hypothesis, we assessed whether a combination of PARPi (olaparib), with or without IR, induces significant increases in levels of DNA damage. Elevated γ-H2AX positivity was observed in IHA-IDH1mut compared to IHA-EV at baseline (Fig. 1, D and E). The differential DDR abilities in IHA-EV and IHA-IDH1mut were more marked when treated with olaparib, radiation, or the combination of both, leading to differences in the amount of unrepaired DSB (Fig. 1, D and E). IDH mutation was associated with a markedly reduced ability to repair DNA damage from IR and PARPi, as measured by the neutral Comet assay (Fig. 1, F and G). The combination of IR and PARPi displayed a cooperative effect. Moreover, the deficiency in DDR found in IHA-IDH1mut cells leads to a greater extent of cell death when treated with the combination as shown by annexin V flow cytometry (Fig. 1, H and I).

Mechanistic studies show that PARPis can be classified on the basis of their ability to trap PARP proteins to DNA, thus preventing the recycling of PARP (*24*). Olaparib has potent PARP trapping activity and consequential cytotoxicity (*21*). However, treatment with strong PARP-trapping agents, such as olaparib and talazoparib, tends to confer resistance through genetic mutation (*25*, *26*). Veliparib has demonstrated weaker trapping activity but strong inhibition of PARylation, effecting an alternative type of mechanistic target manipulation (*27*). In addition, veliparib shows superior penetration through the blood-brain barrier (BBB) (*28*)—a key feature that is important for brain tumor therapeutics. Therefore, we also tested the efficacy of veliparib. Similar to olaparib, IR + veliparib generated a significantly higher level of γ-H2AX foci in IHA-EV treated with 2-HG than IHA-EV without 2-HG receiving the same IR + veliparib treatment (fig. S1, B and C). We next compared the clonogenic ability of IHA in response to increasing doses of radiation [0, 1, 2, and 4 gray (Gy)] with or without 20 μM veliparib. Under all IR conditions, IHA-EV yielded modest reduction of colonies when simultaneously treated with veliparib, while this reduction was markedly enhanced in IHA-IDH1mut (Fig. 1J and fig. S1D). Similar to our results with veliparib, IHA-IDH1mut showed enhanced sensitivity toward IR when treated with olaparib (fig. S2A). Moreover, we tested the clonogenic ability of two glioma stem cell (GSC) lines, TS543 [IDH wild-type (IDHwt)] and TS603 (IDH1mut), which provide a more clinically relevant model. TS603 GSC also showed notably amplified synthetic lethality when treated with IR and olaparib (fig. S2B). These results indicate that IR + PARPi preferentially inhibits the clonogenic growth of IDH-mutant cells.

Cooperativity between radiation and PARPi in IDH-mutant ICC in vitro

We tested whether the synthetic lethality conferred by PARPi in the setting of mutant IDH is observed in other tumor types that commonly harbor *IDH* mutations. ICC is a highly lethal malignancy with a 5-year overall survival (OS) rate of less than 20% (*29*). The current standard of care for most patients with unresectable disease at presentation is still limited to standard chemotherapy and radiation with median overall survival of only 7 to 12 months and no currently available targeted therapy (*30*–*32*). Genomic studies have observed that a substantial portion of ICCs harbor mutations in *IDH* genes (*3*, *33*). We tested whether expression of mutant IDH1 sensitizes ICC cancer cells to PARPis. First, we expressed IDH1-R132H in a human cholangiocarcinoma cell line (HUCCT1) that is wild type for *IDH*. The expression of mutant IDH1 was confirmed by Western blot (Fig. 2A). Similar to what we observed in the IHA isogenic cell lines, IDH1mut expression significantly increased γ-H2AX positivity. This increase was amplified by olaparib, IR, and the combination treatment (Fig. 2, B and C). The unrepaired DSBs, in turn, led to increased fragmentation of genomic DNA shown by Comet assays (Fig. 2, D and E). Clonogenic capacity of HUCCT1 cells was severely decreased by IDH1mut expression, demonstrated by a 100-fold difference in clonogenicity when IDH1mut HUCCT1 cells were exposed to 6-Gy radiation and 4 μM olaparib (Fig. 2, F and G). In addition, using patient-derived ICC cell lines of

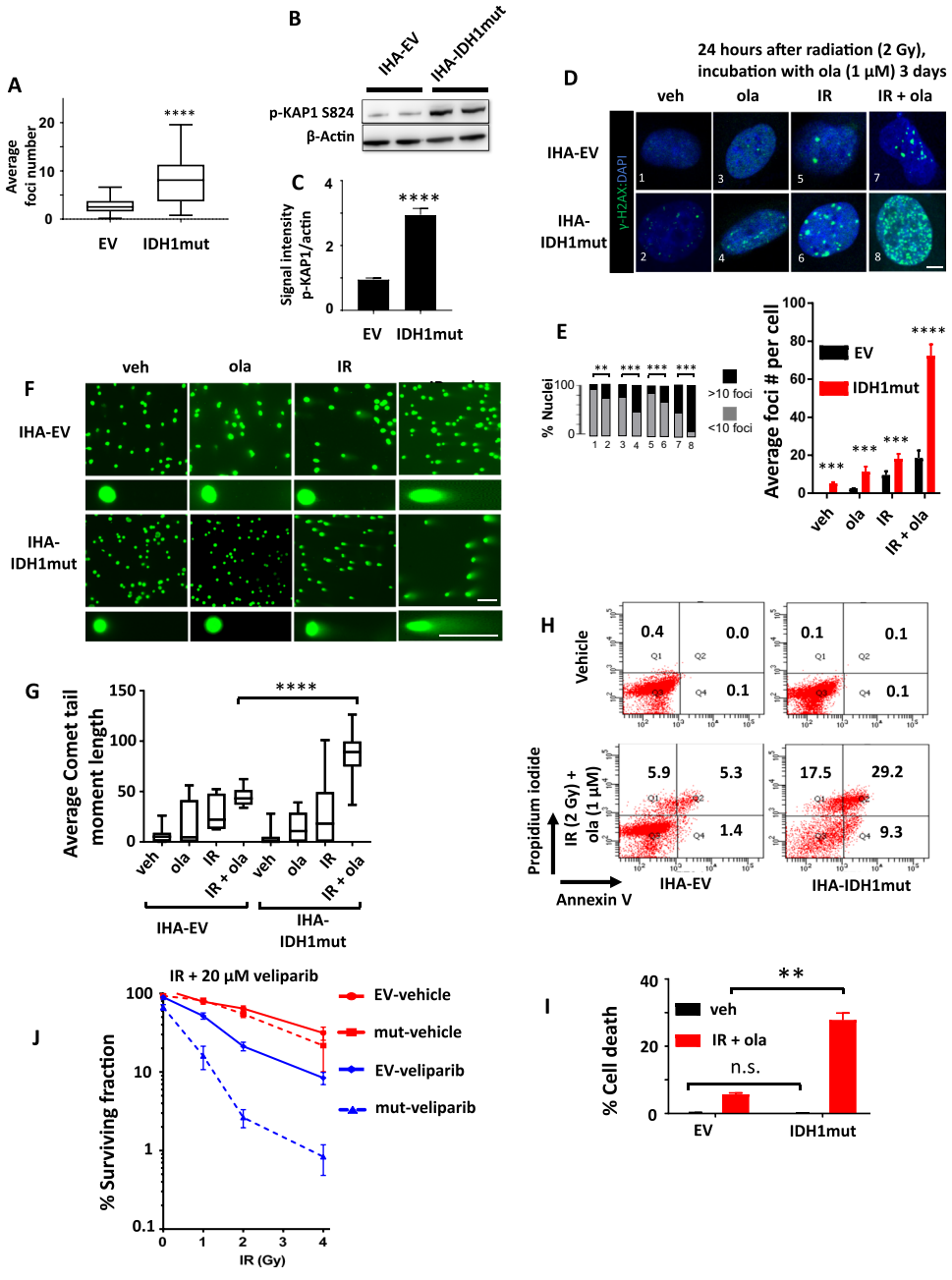

Fig. 1. Mutant IDH1 induces DNA damage response and radiosensitizes IHA to PARP inhibition. (**A**) Quantification of γ-H2AX positivity based on the number of foci. Fifty nuclei were quantified under each condition. (**B**) Western blots of phospho-KAP1 (p-KAP1) and the loading control (β-actin). Samples were loaded in duplicates. (**C**) Relative intensity of each condition in (B) was quantified and plotted. (**D**) Immunostaining of γ-H2AX in vehicle (veh)–, olaparib (ola)–, IR-, or IR + olaparib–treated IHA cells expressing either EV or IDH1mut. DAPI, 4′,6-diamidino-2-phenylindole. Scale bar,10 μm. (**E**) Quantification of (D), performed by measuring the percentage of nuclei with more than 10 foci (left) (the numbers at bottom of bar graphs are correspondent to numbers in the panel) or average foci number of 50 nuclei (right). (**F**) Neutral Comet assays determining DNA breaks in IHA-EV and IHA-IDH1mut. Scale bars, 200 μm. (**G**) The length of comet tails was measured and represented on the plot. (**H**) Apoptotic activities of IHA after radiation and/or olaparib treatment were measured for annexin V and propidium iodide (PI) positivity. (**I**) The PI^+ and annexin V^+ double positive populations were plotted on the bar graph. (**J**) IHA, expressing EV or IDH1mut, was subjected to soft agar colony formation assay, treated with four conditions: vehicle, veliparib (20 μM), IR [1 to 4 grays (Gy)], or IR + veliparib in combination. Plot showed radiosensitization by veliparib in IDH1mut IHA versus EV. Where applicable, error bars represent the SEM. *P* values were determined by Student's *t* test and represented using $^{**}P < 0.01$, $^{***}P < 0.001$, and $^{****}P < 0.0001$. n.s., not significant.

IDHwt (HUCCT1) and IDH1-R132C (SNU-1079), we showed different levels of γ-H2AX staining (Fig. 2H) and clonogenicity (Fig. 2, I and J) in response to IR and olaparib, consistent with the other in vitro models tested above. Together, we showed in two different cancers, using both engineered isogenic cells and native IDH-mutant tumor cell lines, that mutant IDH1 expression leads to hypersensitivity to PARPi, and this hypersensitivity is markedly amplified by radiation.

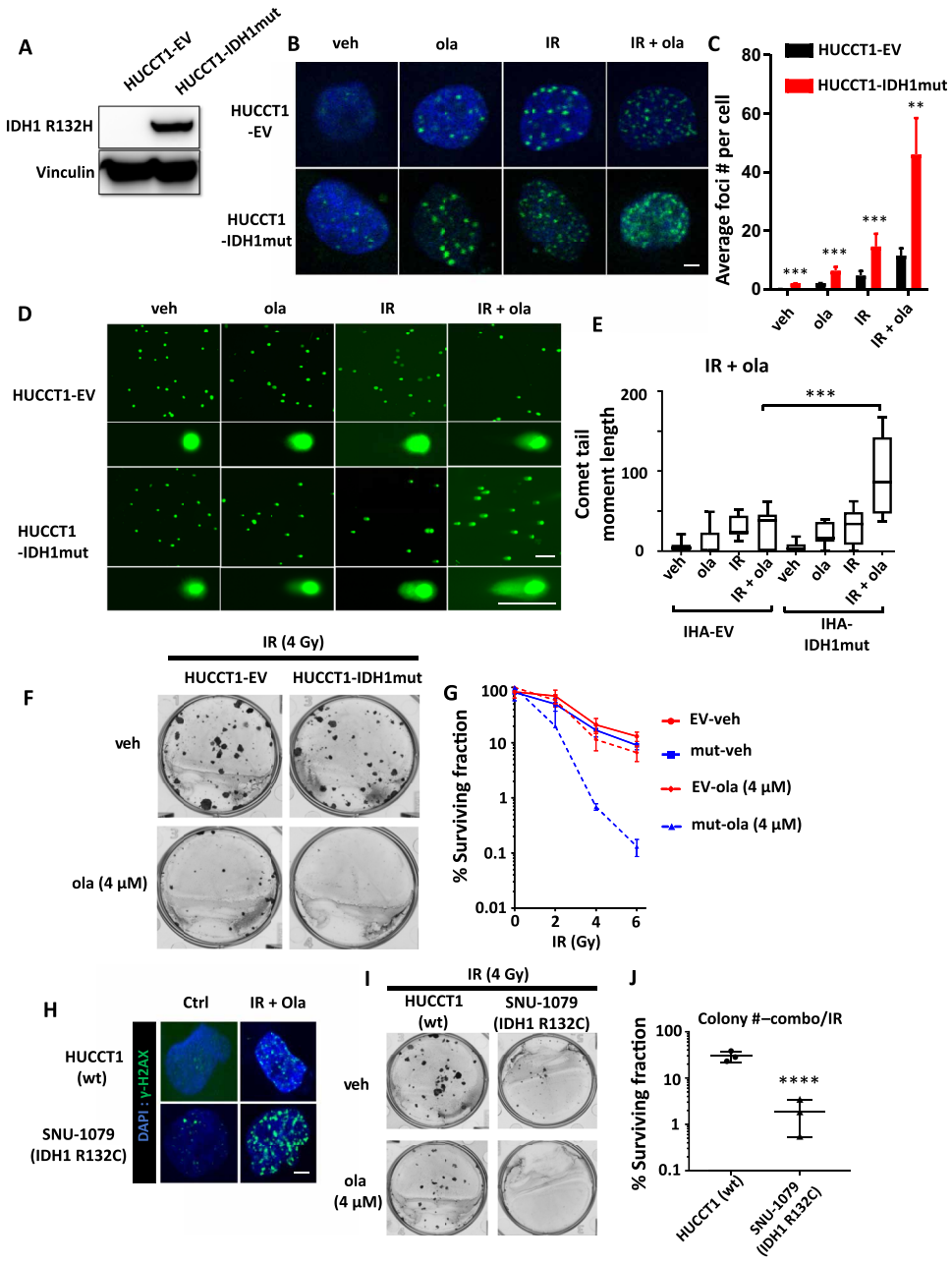

Fig. 2. IDH1-mutant cholangiocarcinoma and sensitivity to PARP inhibition. (**A**) Confirmation of IDH1mut expression in HUCCT1 cholangiocarcinoma cell line. Lysates from HUCCT1-EV or HUCCT1-IDH1mut were subjected to Western blots determining expression of IDH1 R132H. Loading control is performed with anti-vinculin. (**B**) Immunostaining of γ-H2AX in HUCCT1-EV and HUCCT1-IDH1mut after IR (4 Gy) or olaparib (4 μM), or both, showing synergy specifically in HUCCT1-IDH1mut. Scale bar, 10 μm. (**C**) The average number of γ-H2AX foci in (B) were quantified and shown as means ± SEM. (**D**) Neutral Comet assays showed different levels of DNA damage between the indicated treatments. Scale bars, 200 μm. (**E**) The Comet tail moment lengths were individually quantified and compared. (**F**) Representative results of colony formation assay with HUCCT1-EV or HUCCT1-IDH1mut treated with increasing doses of IR (2, 4, and 6 Gy), with or without olaparib (4 μM). (**G**) The colonies of all conditions were quantified and represented on a survival plot showing synergestic effect of olaparib and IR specifically in HUCCT1-IDH1mut cells. Photo credit: Yuxiang Wang, Memorial Sloan Kettering Cancer Center (MSKCC). (**H**) Immunostaining of γ-H2AX in IDHwt (HUCCT1) and IDH1mut (SNU-1079) cell lines, treated with IR (4 Gy) + olaparib (4 μM). wt, wild-type. (**I**) Results from clonogenic assays with IDHwt (HUCCT1) and IDH1mut (SNU-1079) cholangiocarcinoma cell lines. Panel shows representative results when cells were treated with IR (4 Gy) + olaparib 4 μM. Photo credit: Yuxiang Wang, MSKCC. (**J**) The colonies in IR (4 Gy) + olaparib (4 μM) were quantified and divided by the IR-alone control. *P* values were determined by Student's *t* test and represented using $^{**}P < 0.01$, $^{***}P < 0.001$, and $^{****}P < 0.0001$.

Elevated levels of DNA damage in IDH-mutant LGG and ICC patient specimens

Having confirmed that expression of mutant IDH1 is associated with increased levels of DNA damage in vitro, we sought to ascertain whether this is true in patient tumors. We took primary LGG and ICC specimens from patients who underwent surgical resection at Memorial Sloan Kettering Cancer Center (MSKCC) without any previous treatment. With assistance from expert clinical pathologists

at MSKCC, we determined the *IDH* mutation status of the tumors and ensured that the IDH-mutant and wild-type tumors were matched for similar disease stage, grade, and pathologic features. We then subjected the paired tissue samples to γ-H2AX staining, a marker for DNA damage. IDH1mut World Health Organization (WHO) grade III glioma sections showed elevated γ-H2AX signals compared to their IDHwt controls, regardless of their histopathologic classification as oligodendroglioma or astrocytoma (Fig. 3, A and B). Similarly, ICC tumor pairs collected at similar disease stage (T1, no lymph node or distant metastases, no neoadjuvant therapy, and no intrahepatic therapy before resection) demonstrated that *IDH* mutations lead to significantly augmented γ-H2AX staining (Fig. 3, C and D).

Effectiveness of radiation and PARPi for treatment in mouse models of IDH-mutant glioma

Next, we used several animal models to experimentally test our therapeutic approach for IDH-mutant tumors in vivo. First, we intracranially implanted glioma tumorsphere lines (TS543 and TS603) and monitored the tumor growth with bioluminescent imaging (BLI). Mice with tumors were randomized into four-armed trials: control, veliparib (25 mg/kg; 5 days per week until moribund), fractionated RT (2 Gy × 5 fractions, days 1 to 5) or the combination of RT and veliparib (Fig. 4A). Veliparib was used here because of its ability to cross the BBB. Intracranial tumor growth was followed using weekly BLI, and mice were also monitored for OS. Mice with TS543 (IDHwt) tumors showed similar OS in veliparib and control groups (median OS, 11 days versus 10 days) (Fig. 4B), and while RT successfully prolonged OS (median, 19 days) compared to control, the addition of veliparib did not prolong OS (median, 17 days) (Fig. 4B). However, the IDH1mut tumors (TS603) showed significant improvement of OS in veliparib treated group (11 days) compared to control (8.5 days), as well as in RT + veliparib (21 days) versus RT alone (14 days) (Fig. 4C). At day 7 (2 days after the last RT dose), 11 of 16 mice bearing TS603 implantation that received RT and veliparib treatment had reduction in BLI signal, among which 4 of 16 mice showed marked reduction of >90% (Fig. 4, D to F), whereas only 3 of 13 mice receiving RT alone showed reduction and no mice showed >90% reduction (Fig. 4, D to F). In addition, 3 of 13 mice in the RT arm showed BLI signal increase of >800%, while none in the RT + veliparib arm showed this level of tumor growth (Fig. 4, E and F). These

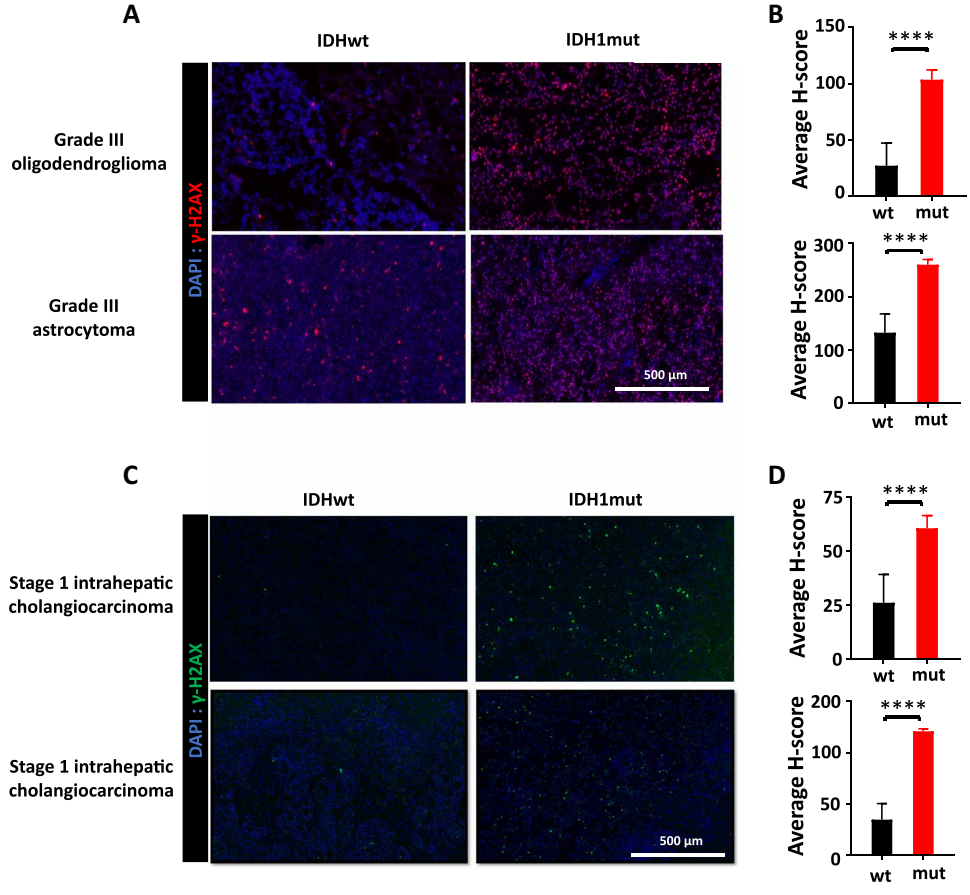

Fig. 3. Human IDH-mutant glioma and cholangiocarcinoma tumors display elevated DDR levels. (**A**) Frozen glioma specimens were collected during routine surgeries at MSKCC (see also the "Human pathology" section under Materials and Methods). Four grade III oligodendroglioma (top) and six grade III astrocytoma (bottom) samples were stained for γ-H2AX positivity, and representative images are shown in the panels. (**B**) H-scores of five 20× fields of each sample were calculated and reported on the bar graphs as means ± SEM. Top: Comparison of H-scores of the oligodendroglioma sample pair. Bottom: Comparison of H-scores of the astrocytoma sample pair. ****$P < 0.0001$, determined by Student's *t* test. (**C**) Sections from six cholangiocarcinoma specimens (three IDHwt and three IDHmut) were stained for γ-H2AX positivity, and representative images are shown in the panels. (**D**) Top: For top panels of (C), H-scores of five 20× fields of each sample were calculated and represented on the bar graphs as means ± SEM. Bottom: Comparison of H-scores of the bottom panels in (C). ****$P < 0.0001$, determined by Student's *t* test.

data suggest that combination therapy with veliparib and RT has greater efficacy against glioma than RT alone in the IDH1-mutant setting. Pathologic studies performed with tumor tissues collected at day 6 (18 hours after the last RT dose) supported the idea that synergy between RT and veliparib was specific to the IDH1-mutant context (figs. S3, A to D, and S4) as shown by quantification of mitotic index (fig. S3, A and B), apoptosis (cleaved caspase 3; fig. S3, C and D), and DNA damage (γ-H2AX; fig. S4).

To rule out the possibility that the observed sensitivity could be due to different genetic backgrounds (i.e., TS543 and TS603), we performed similar trials in a genetically engineered mouse model of glioma with RCAS-TVA (replication competent avian sarcoma-leukosis virus long terminal repeat with a splice acceptor)–mediated gene transfer of mutant IDH in an isogenic setting (*34*, *35*). This is a previously established model where mutant IDH is expressed in endogenously generated gliomas. In these animal models, tumors that express the wild-type or mutant IDH1 were generated through intracranial injection of DF1 cells that carry the corresponding expression cassette (Fig. 5A). The brain tumors were allowed to grow for 5 weeks before magnetic resonance imaging (MRI) scans (Fig. 5A). After the initial MRI scan, the mice were randomized to one of four treatment arms testing tumor sensitivity to veliparib and radiation with MRI scans every week for follow-up (Fig. 5A). The data showed that IDHwt gliomas are sensitive to radiation but relatively insensitive to PARPi, either as monotherapy or in combination with RT (Fig. 5B). On the contrary, IDH1mut gliomas are somewhat sensitive to both RT or veliparib as monotherapy (median OS, 22 days versus 22 days versus 14 days for vehicle control) and the combination of RT and veliparib substantially extended OS (median, 66 days, >4-fold longer OS than vehicle control and 3-fold longer than RT or veliparib alone) (Fig. 5C). Representative MRI images of IDH1mut gliomas show similar initial sizes (Fig. 5D, circled areas) and demonstrate that veliparib limited the tumor growth compared to vehicle-treated tumors (Fig. 5D). Combination treatment with RT and veliparib was able to achieve marked tumor regression over time with some tumors undergoing reduction in tumor size so that they became undetectable at 3 weeks from the start of treatment (Fig. 5D).

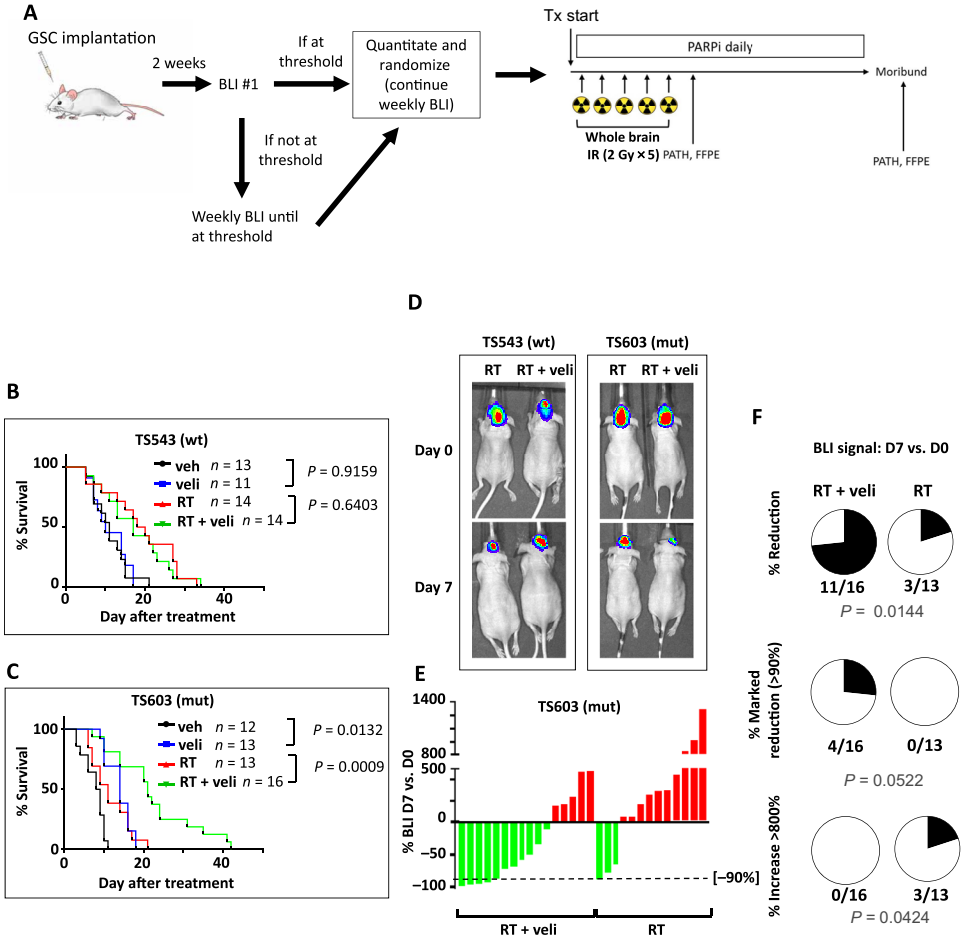

Fig. 4. Treatment with PARPi and RT significantly improved survival of mice with IDH-mutant neurosphere-derived intracranial tumors. (**A**) Work flow of treatments. Mice received GSC implantation. All mice received weekly BLI scans, and the results were recorded. All mice with established tumors (over the defined threshold) were equally distributed to vehicle, veliparib (veli), RT, or RT + veliparib arms. TX, treatment; PATH, pathologic analysis. (**B**) Kaplan-Meier analysis of mice bearing TS543 GSC (IDHwt) cells, starting from the day they entered trials. *P* values were determined by log-rank (Mantel-Cox) test. (**C**) Kaplan-Meier analysis of mice bearing TS603 GSC (IDH1mut), starting from the day they entered trials. (**D**) Representative BLI scans of paired mice receiving RT or RT + veliparib. Top: BLI scans at day 0. Bottom: Scans at day 7. (**E**) Responses based on BLI reads for RT + veliparib–treated (left) ($n = 16$) and RT-treated (right) ($n = 13$) mice. Dashed line indicates a 90% reduction in tumor BLI signal. (**F**) Pie graphs showing the percentage of any reduction (top), >90% reduction (middle), or increase of >800% (bottom) in BLI. Statistics were performed with chi-square test, and the *P* values are presented. D, day.

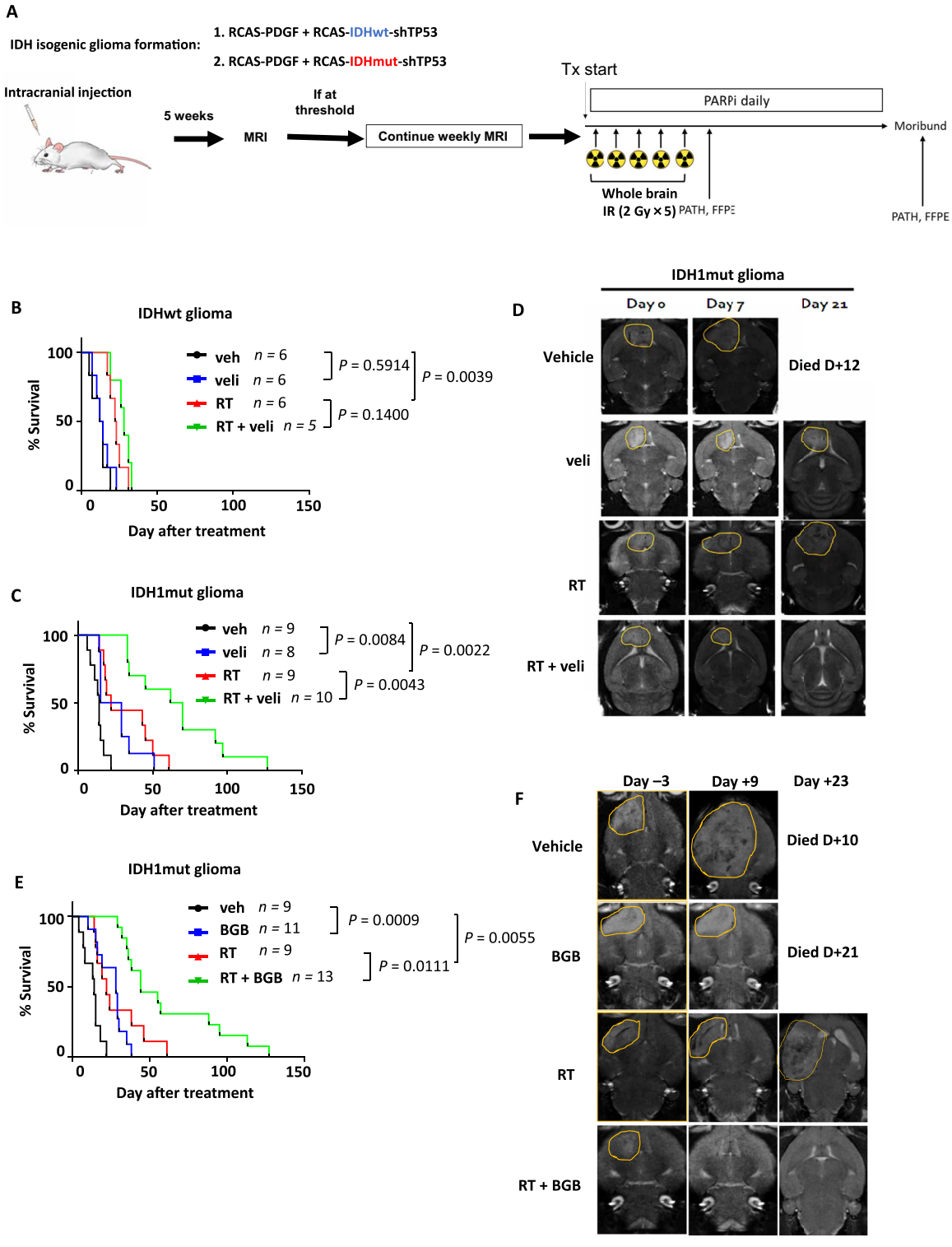

Fig. 5. PARPi + RT significantly improves survival of RCAS-TVA mice bearing mutant IDH1 gliomas. (**A**) Mice receiving intracranial injection of RCAS virus-producing cells carrying platelet-derived growth factor A (PDGFA), shTP53, and either IDHwt or IDHmut expression cassettes were maintained for 5 weeks before their initial MRI scans. After MRI, mice were equally distributed into four-arm treatment groups based on tumor volume. (**B**) Kaplan-Meier analysis of mice bearing IDHwt gliomas, starting from the day they entered trials. *P* values were determined by log-rank (Mantel-Cox) test. (**C**) Kaplan-Meier analysis of mice bearing IDH1mut gliomas. (**D**) Representative images of MRI scans from (C) at days 0, 7, and 21, showing overall effect of treatments. (**E**) Kaplan-Meier analysis of mice bearing IDH1mut gliomas, receiving BGB PARPi + RT treatments. (**F**) Representative images of MRI scans from (E) at days 0, 7, and 21, showing overall effect of treatments.

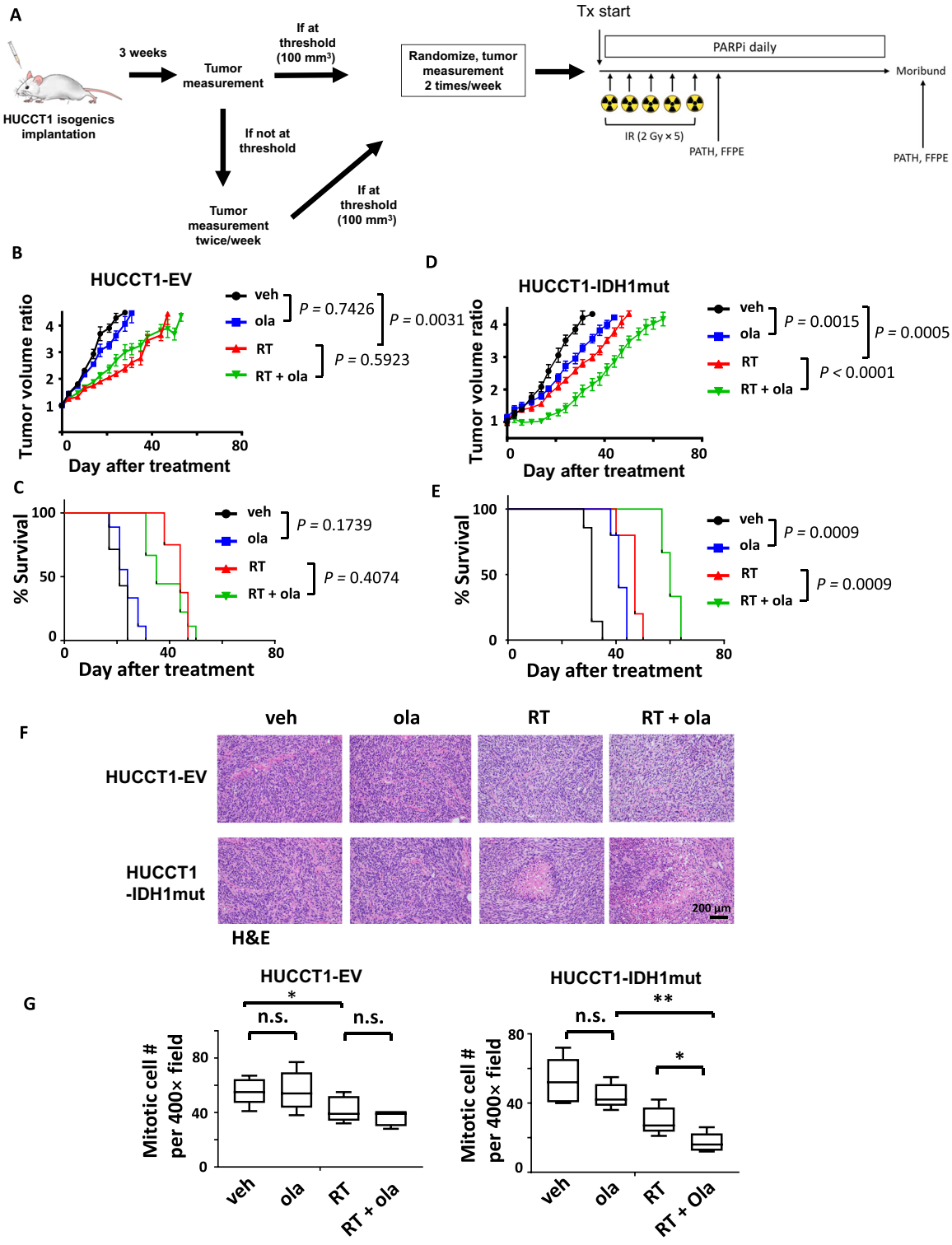

Fig. 6. PARPi + RT significantly improved survival of nude mice bearing IDH1-mutant cholangiocarcinoma xenografts. (**A**) Mice received subcutaneous injection of HUCCT1 cells expressing EV or IDH1mut. Three weeks after injection, the hind flank tumors were measured and equally distributed to four-arm treatment groups when tumors exceeded the defined threshold of 100 mm^3. The tumor sizes were measured twice a week. (**B**) Tumor growth of HUCCT1-EV xenografts with the indicated treatments. *P* values were calculated using two-way ANOVA. (**C**) Kaplan-Meier analysis of HUCCT1-EV xenografts with the indicated treatments. *P* values were determined by log-rank (Mantel-Cox) test. (**D**) Tumor growth of HUCCT1-IDH1mut xenografts with the indicated treatments. (**E**) Kaplan-Meier analysis of HUCCT1-IDH1mut xenografts. (**F**) Mice were sacrificed at day 6, and tumor tissues were subjected to pathological analyses. Hematoxylin and eosin (H&E) staining was performed. (**G**) The mitotic cell numbers per 400× field were counted, and means ± SEM was shown on the bar graphs. For each condition, 10 400× fields were quantified. *$P < 0.05$ and **$P < 0.01$. *P* values were determined by Student's *t* test.

BGB-290 (Pamiparib) is a potent PARPi with good oral bioavailability and excellent BBB penetration (*36*). In contrast to veliparib, BGB-290 displayed potent PARP-trapping activity at nanomolar level (*36*). Thus, we also tested BGB-290 in our RCAS-IDH glioma model. BGB-290 prolonged the OS of mice with IDH1mut glioma, both as monotherapy (median OS, 28 days) or in combination with RT (median OS, 44 days), with 4 of 13 mice living more than 90 days (Fig. 5E). MRI also showed decelerated tumor growth in the BGB-290–treated group and marked reduction of tumor volume in the RT + BGB-290 group (Fig. 5F). Histopathologic studies showed reduced mitotic activity (fig. S5, A and B), as well as increased apoptotic activity (fig. S5, C and D) and accumulation of DSB (fig. S6) specifically in veliparib- and BGB-290–treated tumors. Again, these findings suggest cooperativity between PARPi and radiation in the setting of IDHmut tumors.

Targeting mutant IDH ICC in vivo

Last, we tested our synthetic lethal approach in the context of IDH-mutant ICC in vivo using an animal model. As shown above (Fig. 2, H to J), the IDH1-mutant SNU-1079 ICC line showed increased sensitivity to olaparib. Unfortunately, none of the mice (n = 40) that received subcutaneous injection of SNU-1079 cells developed detectable tumor after 3 months, making it impossible to test the effect of PARPi on this ICC cell line in vivo. However, HUCCT1 cells competently form subcutaneous tumors in athymic nude mice regardless of the mutational status of *IDH1*. Therefore, we subcutaneously implanted isogenic IDHwt and IDH1mut tumors in the hind flank region and treated mice with vehicle, olaparib, RT, or RT + olaparib (Fig. 6A). The IDH1mut tumors grew slightly slower than the wild-type tumors (median survival, 31 days versus 21 days; Fig. 6, B and D), consistent with previously reported 2-HG toxicity. Measurements of tumor volume over time showed that the IDH1wt tumors are insensitive to olaparib treatment. Moreover, although RT slowed down tumor growth, addition of olaparib failed to further delay tumor growth (Fig. 6, B and C). However, the HUCCT1-IDH1mut tumors grew slower when treated with olaparib alone (median time to reach four times initial tumor volume, 41 days versus 31 days). Moreover, RT and olaparib treatment (median OS, 60 days) significantly delayed growth compared to RT alone (median OS, 47 days) (Fig. 6, D and E). Histopathologic analyses with tumor tissues collected at day 6 showed, specifically in IDH1mut tumors, greater reduction in mitotic index (Fig. 6, F and G), increase in apoptosis (fig. S7A), reduction in Ki-67 positivity (fig. S7B), and increase in DSB (fig. S7C). Together, these in vivo findings support, in ICC cells, that *IDH* mutations confer vulnerability to PARPi, which can be further exploited by introducing DNA damaging agents, such as radiation.

DISCUSSION

Despite current standard-of-care multimodal treatment approaches for glioma, including surgery, radiation, and chemotherapy, the outcomes for these patients remain poor (*37*). The case for ICC is similar, and researchers have struggled to find effective targeted therapies with none standardly in clinical use for these diseases at the present time. The low patient survival is multifactorial but likely stems from the similar clinical challenges presented by LGG and ICC. Both diseases occur in critical organs, often cannot be completely resected, tend to recur locally, and commonly cause death through local progression. Furthermore, both diseases have complicated tumor microenvironments and heterogenicity predisposing to therapeutic resistance. Although directly targeting the mutant IDH enzyme with small-molecule inhibitors has been shown to have benefits in patients with AML, concerns exist regarding their application to solid tumors, such as systemic availability of the drug, ability to penetrate into tumor, and lack of efficacy. In vitro studies of IDH1 inhibitor AGI-5027 have failed to show increased sensitivity in IDH1mut versus IDH1wt ICC cells (*38*). Moreover, in solid tumors, mutation of *IDH* typically portends a better prognosis compared to tumors with wild-type *IDH*. This has been shown to be the case for both glioma (*2*) and ICC (*4*), which begs the question of whether targeting the IDH phenotype for reversal makes sense. We examine an approach to treating IDHmut tumors that takes advantage of their unique metabolic, genomic, and epigenetic state through exploitation of impaired HR associated with mutations in *IDH1*. While a randomized phase 1/2 study of temozolomide (TMZ) ± veliparib showed no benefit in recurrent TMZ-refractory glioblastoma, *IDH* mutation status was not considered in the enrollment criteria nor reported in the manuscript (*39*). To our knowledge, combined treatment with PARPi + RT has not been examined in the specific setting of IDH-mutant tumors at either the laboratory or clinical level.

We developed both in vitro and in vivo models that mimic IDH-mutant tumors found in the patients. Using these models, we were able to determine that *IDH* mutation confers sensitivity to DNA damaging agents and PARP inhibitors, and we established preclinical strategies to target these therapeutic vulnerabilities. Most LGG recurrences (up to 92%) occur within the RT field (*40*). Our results nominate PARPi-based systemic therapy as a way to increase control of IDHmut gliomas. We hypothesize that combination therapy with PARPi + RT, as evaluated in our study, could substantially lengthen OS and progression-free survival for patients with IDHmut LGG. In the setting of ICC, unresectable and recurrent intrahepatic disease poses an imminent threat to patient lives, given their proclivity to cause liver failure through biliary, portal vein, or hepatic vein obstruction. Nonoperative therapies produce median OS of only 7 to 12 months (*31*, *41*). Conventional RT doses, even with concurrent chemotherapy, achieve only modest improvement in outcomes and few long-term survivors (*32*) with most patients experiencing local progression as site of first failure (*42*). Similar to LGGs, given the propensity of ICCs to cause death through local progression, the ability to further increase tumor cell killing within the RT field for unresectable and recurrent intrahepatic disease through combined PARPi + RT in the IDHmut setting can be explored.

Ongoing clinical trials have been set up to test this concept (e.g., NCT03212274, NCT03561870, NCT03749187, etc.), yet the strategies and designs of these trials still lack critical rationale or insights from preclinical studies. For example, in our animal studies, PARPi alone, whether it is veliparib, BGB-290, or olaparib, provided modest benefit for OS. Yet, the combination with radiation markedly amplified this benefit. Our data suggest that concurrent RT needs to be considered to yield maximal benefit of PARPi therapy for IDHmut tumors. While the mechanisms underlying this are still being worked out, Sulkowski *et al.* (*16*) show that 2-HG–dependent inhibition of KDM4A and KDM4B may contribute to the observed synthetic lethality. These two proteins are key αKG-dependent histone demethylases that are important for proper DNA damage response. Our study suggests that these biological phenomena may potentially be clinically actionable and should be tested.

MATERIALS AND METHODS

Study design

The objective of this study was to determine the therapeutic efficacy of PARPis, as monoagent or in combination with IR, for IDH-mutant tumors. This was a controlled, laboratory-based, experimental study using cell line models in culture, tumor specimens, tumor cell xenograft, and genetically engineered mouse models. Isogenic cell lines and genetically engineered tumors were produced by introducing mutant IDH1, along with appropriate controls. IDHwt and IDHmut patient-derived glioma and cholangiocarcinoma cell lines were compared and provided additional, disease-related evidence. Randomization of animals varied depending on individual assays and is described separately below. Pharmaceutical agents against PARP and/or IR were applied. Sample sizes were determined independently for each experiment without formal power calculation. No data were excluded from analyses. Unless otherwise specified, experiments used three replicates per sample. End points varied by experiment and are described below, in figure legends, or in Results. Histopathological and immunohistochemical review of xenografts was conducted by pathologist (C.S., D.S.K., and J.T.H.) in a nonblinded fashion. Quantification of mitotic index, γ-H2AX, Ki67 and cleaved caspase 3 immunostaining, length of Comet tails, colony numbers, and BLI signals was blinded.

Reagents

The source of antibodies, chemicals, plasmids, cell lines, and mouse strains used in this study are listed in table S1.

Cell culture

All cell lines used in this study were regularly tested for mycoplasma contamination at the Antibody and Bioresource Core of MSKCC. Parental IHAs (a gift from R. O. Peiper, University of California, San Francisco) were infected with a viral vector carrying expression cassette for IDH1-R132H or the empty vector control (*10*). TS543 and TS603 are patient-derived GSCs (*43*–*45*) maintained in NeuroCult NS-A Proliferation media (no. 05751, STEMCELL Technologies). For intracranial injection, TS543 or TS603 was infected with pHIV-Luc-ZsGreen (a gift from B. Welm; no. 39196, Addgene) and fluorescence-activated cell sorting–sorted for top 10% ZsGreen expression. Two well-characterized patient-derived human ICC cell lines were obtained as follows: (i) SNU-1079 (endogenous R132C mutation in *IDH1*) was purchased from the Korean Cell Line Bank (Cancer Research Institute, Seoul National University, Seoul, Korea; http://cellbank.snu.ac.kr), and (ii) HUCCT1 was purchased from the RIKEN BioResource Research Center Cell Bank (Tsukuba, Japan; https://en.brc.riken.jp/). To generate HUCCT1 isogenic cells, the parental HUCCT1 cells were infected with pLNCX2 retroviruses expressing IDH1-R132H or the empty vector control (*7*). Olaparib (no. S1060) and veliparib (no. S1004) were purchased from Selleckchem. BGB-290 (no. C-1286) was purchased from Chemgood. For in vitro use, olaparib, veliparib, and BGB-290 were diluted with dimethyl sulfoxide (DMSO). For in vivo use, olaparib was diluted with DMSO as a stock and further diluted with 10% (w/v) 2-hydroxy-propyl-β-cyclodextrin (no. H107, Sigma-Aldrich). Veliparib and BGB-290 were diluted with DMSO and further diluted with phosphate-buffered saline (PBS). The final solutions were prepared fresh before each injection. For 2-HG treatment, Octyl-D-2-HG (no. 16366, Cayman Chemical, MI) was initially diluted into DMSO and further diluted with culture medium to achieve a final concentration of 1 mM.

Mice

All mouse experiments were approved by Institutional Animal Care and Use Committee at MSKCC strictly following its guidelines. Female nude mice (age 4 to 6 weeks) were purchased from Taconic Biosciences and maintained in the xenograft suite. *Nestin-TVA* mice were obtained from E. Holland (Fred Hutchinson).

Human pathology

All tumors were obtained following surgical resection at the MSKCC as part of routine clinical care in accordance with the Institutional Review Board policies at the MSKCC. Informed consent was obtained from all patients. Ten glioma (five wild-type and six mutant) and six cholangiocarcinoma (three wild-type and three mutant) samples were included in this study. The clinical determination, classification, and grouping were performed by pathologists at MSKCC and MD Anderson. For glioma patient samples, 10-μm sections of frozen tissues was directly fixed with 4% paraformaldehyde in PBS for 30 min, followed by staining procedures as described below in the "Immunofluorescent imaging" section. For cholangiocarcinoma patient samples, formalin-fixed paraffin-embedded (FFPE) sections were stained following antigen retrieval with boiling citrate buffer (10 mM) (pH 6), following procedures in the "Immunofluorescent imaging" section. After staining, the sections were scanned with Pannoramic 250 (3DHISTECH, Budapest, Hungary) using Zeiss 20×/0.8 numerical aperture objective. The scans were viewed and exported to .tif images using CaseViewer software (3DHISTECH, Budapest, Hungary). γ-H2AX positivity was quantified as H-score ($1 \times A + 2 \times B + 3 \times C$), where A is the percentage of cells with no staining, B is the percentage of cells with weak to moderate staining, and C is the percentage of cells with strong staining. The quantification was performed by the Molecular Cytology Core, and the score determination was double checked by Y.W.

Clonogenic assays

For soft agar colony formation assays, 50,000 cells were seeded in six-well plates containing 1% bottom layer and 0.5% top layer soft agar. Cells were then cultured in growth media with or without olaparib (1 μM) or veliparib (20 μM). Radiation dosing of 0, 1, 2, or 4 Gy was immediately applied after plating. The 1.5 ml of growth media covering the agar cultures was replenished every week. At day 21, colonies were fixed with 4% paraformaldehyde for 30 min and stained with 0.005% crystal violet in PBS overnight. Stained colonies were then washed extensively in PBS and water and quantified on a GelCount colony counter (Oxford Optronix).

Clonogenic assays were performed by plating cells in exponential growth phase at 125 to 1000 cells per 10-cm dish depending on the radiation dose level. Olaparib (4 μM) was added 24 hours after plating with IR (0 to 6 Gy) delivered 24 hours later. Colonies (>50 cells) were counted with GelCount colony counter (Oxford Optronix) 10 to 14 days after IR by fixing and staining with a solution of 0.1% crystal violet in 4% paraformaldehyde in PBS. Surviving fraction was calculated by dividing colonies by cells plated with adjustment for plating efficiency.

Comet assays

Comet assays were performed using OxiSelect Comet Assay Kit (STA-350, Cell Biolabs) according to the manufacturer's instruction. Briefly, cells were mixed with agarose, dropped onto the glass slides provided by the kit, and lysed with prechilled lysis buffer for 60 min at

4°C in the dark. The electrophoresis was performed with prechilled tris-borate EDTA buffer, followed by five times washes with ddH_2O. The slides were then incubated in cold 70% ethanol for 5 min and air-dried. Representative pictures were taken with a wide-field microscope with fluorescein isothiocyanate channel (Nikon) and analyzed with OpenComet plug-in in ImageJ (*46*).

Immunofluorescent imaging

Cells were grown in chamber slides (Nunc Lab-Tek II, cat no. 154526, Thermo Fisher Scientific) before fixation (4% paraformaldehyde in PBS for 10 min) and permeabilization (0.5% Tween 20 and 0.2% Triton X-100 in PBS for 10 min). Cells were blocked with goat serum (Sigma-Aldrich) for 4 hours at room temperature and incubated with γ-H2AX antibody (1:500; no. 05-636, Millipore) overnight at 4°C and secondary antibody (1:2000; goat anti-mouse Alexa Fluor 488 or Alexa Fluor 568) for 2 hours. The slides were mounted with coverslips using ProLong Gold antifade reagent and 4′,6-diamidino-2-phenylindole counterstain (Invitrogen).

Bioluminescent imaging

BLI was performed weekly following intraperitoneal injection of D-luciferin (PerkinElmer) and measured using Xenogen IVIS Spectrum in vivo imaging system (PerkinElmer). Living Image software (PerkinElmer) was used to acquire and analyze the BLI data.

Magnetic resonance imaging

Brains of injected mice were scanned on a 200-MHz Bruker 4.7 T Biospec MRI scanner (Bruker Biospin Corp., Ettlingen, Germany) and equipped with a 300-mT/m ID 20-cm gradient (Resonance Research Inc., Billerica, MA). Mice were anaesthetized by 2% isoflurane in oxygen. Sedated animals were physiologically monitored during scan period (SA Instruments Inc., Stony Brook, NY). For mouse brain imaging, brain axial T2-weighted images using fast spin-echo RARE (Rapid Acquisition with Relaxation Enhancement) sequence were acquired by sequential scanning with a slice thickness of 1 mm.

Xenograft of GSC

TS543 or TS603 cells expressing pHIV-Luc-ZsGreen (described above) were implanted into the brain of nude mice (5×10^5 cells per brain), with a fixed stereotactic device (Stoelting, Illinois). Injections were made to the right frontal cortex, 3-mm lateral and 3-mm caudal, and at a depth of 3 mm with respect to bregma. Two weeks after the implantation, the tumor growth is monitored by BLI and MRI once every week, respectively. Tumors over the BLI threshold were correlated with MRI signal for confirmation of location and actual volume. The mice with confirmed tumors enter a randomized trial consists of the following: (i) vehicle; (ii) intraperitoneal injection of veliparib (25 mg/kg, 5 days per week); (iii) RT (2 Gy × 5 fractions), delivered to the whole head using an X-RAD 320 Irradiation Platform (Precision X-Ray Inc., North Branford, CT; www.pxinc.com) in combination with a QUAD Fixture and Shield Set specifically designed with lead shielding of the body to allow for cranial irradiation (Precision X-Ray Inc., Connecticut); and (iv) RT + veliparib (concurrent treatment for the initial 5 days and then veliparib injection 5 days per week). The BLI signals were continuingly followed up weekly until defined end of trial (death). For pathological analyses, three mice of each group were sacrificed at day 6 after the initial trial start, and the brains were collected and subjected to standard FFPE processing.

Genetically engineered glioma mouse model by RCAS viral gene transfer

Nestin-TVA mice were a gift from E. Holland (Fred Hutchinson, Seattle, WA) (*47*). RCAS vectors carrying expression cassette for platelet-derived growth factor A (PDGFA), IDH1wt-shTP53, and IDH1R132H-shTP53 were gifts from E. Holland (*35*). RCAS viral vectors were introduced into DF1 cells separately, and the expression of PDGFA, IDH1wt, and IDH1-R132H was verified by Western blots. Cells expressing PDGFA were mixed with cells expressing IDH1wt-shTP53 or IDH1R132H-shTP53 at a ratio of 1:1 (3×10^5 total) and intracranially injected as described above. Mice received MRI at week 5 after the initial injection, and the tumors were randomized on the basis of size so that tumors of different sizes are equally distributed across groups: (i) vehicle; (ii) intraperitoneal injection of veliparib (25 mg/kg, 5 days per week) or BGB-290 (6 mg/kg, 5 days per week); (iii) RT (2 Gy × 5 days), delivered to the whole head using X-RAD 320 Irradiation Platform; and (iv) RT + veliparib or BGB-290 (concurrent treatment with RT delivered 1 hour after veliparib/BGB-290 injection for the initial 5 days and then veliparib/BGB-290 injection 5 days per week). The MRI signals were followed weekly until defined end of trial (death). For pathological analyses, three mice from each group were sacrificed at day 6 after the initial trial start, and the brains were collected and subjected to standard FFPE processing.

ICC xenograft

HUCCT1 cells expressing IDH1R132H or the empty vector control were harvested at exponentially proliferative stage and mixed 1:1 (v/v) with Matrigel (no. 356231, Corning). A total of 5×10^6 cells were injected into nude mice flanks in a 100-μl volume. The size of tumors was measured with caliber and calculated using the formula $(l \times w^2)/2$, where w is width and l is length in millimeters. Tumors that reached threshold (100 mm^3) were randomized to the following: (i) vehicle; (ii) intraperitoneal injection of olaparib (50 mg/kg, 5 days per week); (iii) RT (2 Gy × 5 days), delivered to the posterior through the X-RAD 320 Irradiation Platform; and (iv) RT + olaparib (concurrent treatment for the initial 5 days and then olaparib injection 5 days per week). The tumor volume was continuingly measured twice a week until the defined end of trial (400 mm^3). For pathological analyses, three mice of each group were sacrificed at day 6 after the initial trial start, and the xenograft tumors were collected and subjected to standard FFPE processing.

Statistical analysis

Statistical analysis was performed using GraphPad Prism 7. Where applicable, P value was determined by unpaired, two-tailed t tests, if not otherwise specified. Difference of tumor growth curves was determined by two-way analysis of variance (ANOVA). Log-rank (Mantel-Cox) test were used to determine the significance of differences in Kaplan-Meier analysis of GSC xenograft, RCAS-induced gliomas, and ICC hind flank xenograft experiments. Unless otherwise stated, all results, representing at least three independent experiments, were plotted as means ± SEM. P values are represented either directly on figures or using $^*P < 0.05$, $^{**}P < 0.01$, $^{***}P < 0.001$, and $^{****}P < 0.0001$.

SUPPLEMENTARY MATERIALS

Supplementary material for this article is available at http://advances.sciencemag.org/cgi/content/full/6/17/eaaz3221/DC1

View/request a protocol for this paper from *Bio-protocol*.

REFERENCES AND NOTES

1. Cancer Genome Atlas Research Network, D. J. Brat, R. G. Verhaak, K. D. Aldape, W. K. Yung, S. R. Salama, L. A. D. Cooper, E. Rheinbay, C. R. Miller, M. Vitucci, O. Morozova, A. G. Robertson, H. Noushmehr, P. W. Laird, A. D. Cherniack, R. Akbani, J. T. Huse, G. Ciriello, L. M. Poisson, J. S. Barnholtz-Sloan, M. S. Berger, C. Brennan, R. R. Colen, H. Colman, A. E. Flanders, C. Giannini, M. Grifford, A. Iavarone, R. Jain, I. Joseph, J. Kim, K. Kasaian, T. Mikkelsen, B. A. Murray, B. P. O'Neill, L. Pachter, D. W. Parsons, C. Sougnez, E. P. Sulman, S. R. Vandenberg, E. G. Van Meir, A. von Deimling, H. Zhang, D. Crain, K. Lau, D. Mallery, S. Morris, J. Paulauskis, R. Penny, T. Shelton, M. Sherman, P. Yena, A. Black, J. Bowen, K. Dicostanzo, J. Gastier-Foster, K. M. Leraas, T. M. Lichtenberg, C. R. Pierson, N. C. Ramirez, C. Taylor, S. Weaver, L. Wise, E. Zmuda, T. Davidsen, J. A. Demchok, G. Eley, M. L. Ferguson, C. M. Hutter, K. R. M. Shaw, B. A. Ozenberger, M. Sheth, H. J. Sofia, R. Tarnuzzer, Z. Wang, L. Yang, J. C. Zenklusen, B. Ayala, J. Baboud, S. Chudamani, M. A. Jensen, J. Liu, T. Pihl, R. Raman, Y. Wan, Y. Wu, A. Ally, J. T. Auman, M. Balasundaram, S. Balu, S. B. Baylin, R. Beroukhim, M. S. Bootwalla, R. Bowlby, C. A. Bristow, D. Brooks, Y. Butterfield, R. Carlsen, S. Carter, L. Chin, A. Chu, E. Chuah, K. Cibulskis, A. Clarke, S. G. Coetzee, N. Dhalla, T. Fennell, S. Fisher, S. Gabriel, G. Getz, R. Gibbs, R. Guin, A. Hadjipanayis, D. N. Hayes, T. Hinoue, K. Hoadley, R. A. Holt, A. P. Hoyle, S. R. Jefferys, S. Jones, C. D. Jones, R. Kucherlapati, P. H. Lai, E. Lander, S. Lee, L. Lichtenstein, Y. Ma, D. T. Maglinte, H. S. Mahadeshwar, M. A. Marra, M. Mayo, S. Meng, M. L. Meyerson, P. A. Mieczkowski, R. A. Moore, L. E. Mose, A. J. Mungall, A. Pantazi, M. Parfenov, P. J. Park, J. S. Parker, C. M. Perou, A. Protopopov, X. Ren, J. Roach, T. S. Sabedot, J. Schein, S. E. Schumacher, J. G. Seidman, S. Seth, H. Shen, J. V. Simons, P. Sipahimalani, M. G. Soloway, X. Song, H. Sun, B. Tabak, A. Tam, D. Tan, J. Tang, N. Thiessen, T. Triche Jr., D. J. Van Den Berg, U. Veluvolu, S. Waring, D. J. Weisenberger, M. D. Wilkerson, T. Wong, J. Wu, L. Xi, A. W. Xu, L. Yang, T. I. Zack, J. Zhang, B. A. Aksoy, H. Arachchi, C. Benz, B. Bernard, D. Carlin, J. Cho, D. DiCara, S. Frazer, G. N. Fuller, J. Gao, N. Gehlenborg, D. Haussler, D. I. Heiman, L. Iype, A. Jacobsen, Z. Ju, S. Katzman, H. Kim, T. Knijnenburg, R. B. Kreisberg, M. S. Lawrence, W. Lee, K. Leinonen, P. Lin, S. Ling, W. Liu, Y. Liu, Y. Lu, G. Mills, S. Ng, M. S. Noble, E. Paull, A. Rao, S. Reynolds, G. Saksena, Z. Sanborn, C. Sander, N. Schultz, Y. Senbabaoglu, R. Shen, I. Shmulevich, R. Sinha, J. Stuart, S. O. Sumer, Y. Sun, N. Tasman, B. S. Taylor, D. Voet, N. Weinhold, J. N. Weinstein, D. Yang, K. Yoshihara, S. Zheng, W. Zhang, L. Zou, T. Abel, S. Sadeghi, M. L. Cohen, J. Eschbacher, E. M. Hattab, A. Raghunathan, M. J. Schniederjan, D. Aziz, G. Barnett, W. Barrett, D. D. Bigner, L. Boice, C. Brewer, C. Calatozzolo, B. Campos, C. G. Carlotti Jr., T. A. Chan, L. Cuppini, E. Curley, S. Cuzzubbo, K. Devine, F. DiMeco, R. Duell, J. B. Elder, A. Fehrenbach, G. Finocchiaro, W. Friedman, J. Fulop, J. Gardner, B. Hermes, C. Herold-Mende, C. Jungk, A. Kendler, N. L. Lehman, E. Lipp, O. Liu, R. Mandt, M. McGraw, R. McLendon, C. McPherson, L. Neder, P. Nguyen, A. Noss, R. Nunziata, Q. T. Ostrom, C. Palmer, A. Perin, B. Pollo, A. Potapov, O. Potapova, W. K. Rathmell, D. Rotin, L. Scarpace, C. Schilero, K. Senecal, K. Shimmel, V. Shurkhay, S. Sifri, R. Singh, A. E. Sloan, K. Smolenski, S. M. Staugaitis, R. Steele, L. Thorne, D. P. C. Tirapelli, A. Unterberg, M. Vallurupalli, Y. Wang, R. Warnick, F. Williams, Y. Wolinsky, S. Bell, M. Rosenberg, C. Stewart, F. Huang, J. L. Grimsby, A. J. Radenbaugh, J. Zhang, Comprehensive, integrative genomic analysis of diffuse lower-grade gliomas. *N. Engl. J. Med.* **372**, 2481–2498 (2015).
2. D. W. Parsons, S. Jones, X. S. Zhang, J. C.-H. Lin, R. J. Leary, P. Angenendt, P. Mankoo, H. Carter, I.-M. Siu, G. L. Gallia, A. Olivi, R. McLendon, B. A. Rasheed, S. Keir, T. Nikolskaya, Y. Nikolsky, D. A. Busam, H. Tekleab, L. A. Diaz Jr, J. Hartigan, D. R. Smith, R. L. Strausberg, S. K. N. Marie, S. M. O. Shinjo, H. Yan, G. J. Riggins, D. D. Bigner, R. Karchin, N. Papadopoulos, G. Parmigiani, B. Vogelstein, V. E. Velculescu, K. W. Kinzler, An integrated genomic analysis of human glioblastoma multiforme. *Science* **321**, 1807–1812 (2008).
3. Y. Jiao, T. M. Pawlik, R. A. Anders, F. M. Selaru, M. M. Streppel, D. J. Lucas, N. Niknafs, V. B. Guthrie, A. Maitra, P. Argani, G. J. A. Offerhaus, J. C. Roa, L. R. Roberts, G. J. Gores, I. Popescu, S. T. Alexandrescu, S. Dima, M. Fassan, M. Simbolo, A. Mafficini, P. Capelli, R. T. Lawlor, A. Ruzzenente, A. Guglielmi, G. Tortora, F. de Braud, A. Scarpa, W. Jarnagin, D. Klimstra, R. Karchin, V. E. Velculescu, R. H. Hruban, B. Vogelstein, K. W. Kinzler, N. Papadopoulos, L. D. Wood, Exome sequencing identifies frequent inactivating mutations in BAP1, ARID1A and PBRM1 in intrahepatic cholangiocarcinomas. *Nat. Genet.* **45**, 1470–1473 (2013).
4. P. Wang, Q. Dong, C. Zhang, P.-F. Kuan, Y. Liu, W. R. Jeck, J. B. Andersen, W. Jiang, G. L. Savich, T.-X. Tan, J. T. Auman, J. M. Hoskins, A. D. Misher, C. D. Moser, S. M. Yourstone, J. W. Kim, K. Cibulskis, G. Getz, H. V. Hunt, S. S. Thorgeirsson, L. R. Roberts, D. Ye, K.-L. Guan, Y. Xiong, L.-X. Qin, D. Y. Chiang, Mutations in *isocitrate dehydrogenase* 1 and 2 occur frequently in intrahepatic cholangiocarcinomas and share hypermethylation targets with glioblastomas. *Oncogene* **32**, 3091–3100 (2013).
5. E. R. Mardis, L. Ding, D. J. Dooling, D. E. Larson, M. D. McLellan, K. Chen, D. C. Koboldt, R. S. Fulton, K. D. Delehaunty, S. D. McGrath, L. A. Fulton, D. P. Locke, V. J. Magrini, R. M. Abbott, T. L. Vickery, J. S. Reed, J. S. Robinson, T. Wylie, S. M. Smith, L. Carmichael, J. M. Eldred, C. C. Harris, J. Walker, J. B. Peck, F. Y. Du, A. F. Dukes, G. E. Sanderson, A. M. Brummett, E. Clark, J. F. McMichael, R. J. Meyer, J. K. Schindler, C. S. Pohl, J. W. Wallis, X. Q. Shi, L. Lin, H. Schmidt, Y. Z. Tang, C. Haipek, M. E. Wiechert, J. V. Ivy, J. Kalicki, G. Elliott, R. E. Ries, J. E. Payton, P. Westervelt, M. H. Tomasson, M. A. Watson, J. Baty, S. Heath, W. D. Shannon, R. Nagarajan, D. C. Link, M. J. Walter, T. A. Graubert, J. F. DiPersio, R. K. Wilson, T. J. Ley, Recurring mutations found by sequencing an acute myeloid leukemia genome. *New Engl. J. Med.* **361**, 1058–1066 (2009).
6. M. F. Amary, K. Bacsi, F. Maggiani, S. Damato, D. Halai, F. Berisha, R. Pollock, P. O'Donnell, A. Grigoriadis, T. Diss, M. Eskandarpour, N. Presneau, P. C. Hogendoorn, A. Futreal, R. Tirabosco, A. M. Flanagan, *IDH1* and *IDH2* mutations are frequent events in central chondrosarcoma and central and periosteal chondromas but not in other mesenchymal tumours. *J. Pathol.* **224**, 334–343 (2011).
7. S. Turcan, D. Rohle, A. Goenka, L. A. Walsh, F. Fang, E. Yilmaz, C. Campos, A. W. Fabius, C. Lu, P. S. Ward, C. B. Thompson, A. Kaufman, O. Guryanova, R. Levine, A. Heguy, A. Viale, L. G. T. Morris, J. T. Huse, I. K. Mellinghoff, T. A. Chan, IDH1 mutation is sufficient to establish the glioma hypermethylator phenotype. *Nature* **483**, 479–483 (2012).
8. C. Lu, P. S. Ward, G. S. Kapoor, D. Rohle, S. Turcan, O. Abdel-Wahab, C. R. Edwards, R. Khanin, M. E. Figueroa, A. Melnick, K. E. Wellen, D. M. O'Rourke, S. L. Berger, T. A. Chan, R. L. Levine, I. K. Mellinghoff, C. B. Thompson, IDH mutation impairs histone demethylation and results in a block to cell differentiation. *Nature* **483**, 474–478 (2012).
9. M. E. Figueroa, O. Abdel-Wahab, C. Lu, P. S. Ward, J. Patel, A. Shih, Y. S. Li, N. Bhagwat, A. Vasanthakumar, H. F. Fernandez, M. S. Tallman, Z. X. Sun, K. Wolniak, J. K. Peeters, W. Liu, S. E. Choe, V. R. Fantin, E. Paietta, B. Löwenberg, J. D. Licht, L. A. Godley, R. Delwel, P. J. M. Valk, C. B. Thompson, R. L. Levine, A. Melnick, Leukemic IDH1 and IDH2 mutations result in a hypermethylation phenotype, disrupt TET2 function, and impair hematopoietic differentiation. *Cancer Cell* **18**, 553–567 (2010).
10. S. Turcan, V. Makarov, J. Taranda, Y. Wang, A. W. M. Fabius, W. Wu, Y. Zheng, N. El-Amine, S. Haddock, G. Nanjangud, H. C. LeKaye, C. Brennan, J. Cross, J. T. Huse, N. L. Kelleher, P. Osten, C. B. Thompson, T. A. Chan, Mutant-IDH1-dependent chromatin state reprogramming, reversibility, and persistence. *Nat. Genet.* **50**, 62–72 (2018).
11. M. D. Amatangelo, L. Quek, A. Shih, E. M. Stein, M. Roshal, M. D. David, B. Marteyn, N. R. Farnoud, S. de Botton, O. A. Bernard, B. Wu, K. E. Yen, M. S. Tallman, E. Papaemmanuil, V. Penard-Lacronique, A. Thakurta, P. Vyas, R. L. Levine, Enasidenib induces acute myeloid leukemia cell differentiation to promote clinical response. *Blood* **130**, 732–741 (2017).
12. C. D. DiNardo, S. De Botton, E. M. Stein, G. J. Roboz, A. S. Mims, D. A. Pollyea, R. T. Swords, J. K. Altman, R. H. Collins, G. N. Mannis, G. L. Uy, W. Donnellan, A. Pigneux, A. T. Fathi, A. S. Stein, H. P. Erba, G. T. Prince, J. M. Foran, E. Traer, R. K. Stuart, M. L. Arellano, J. L. Slack, M. A. Sekeres, K. Yen, S. M. Kapsalis, H. Liu, M. Goldwasser, S. Agresta, E. C. Attar, M. S. Tallman, R. M. Stone, H. M. Kantarjian, Ivosidenib (AG-120) in mutant IDH1 AML and advanced hematologic malignancies: Results of a phase 1 dose escalation and expansion study. *Blood* **130**, (2017).
13. R. Su, L. Dong, C. Li, S. Nachtergaele, M. Wunderlich, Y. Qing, X. Deng, Y. Wang, X. Weng, C. Hu, M. Yu, J. Skibbe, Q. Dai, D. Zou, T. Wu, K. Yu, H. Weng, H. Huang, K. Ferchen, X. Qin, B. Zhang, J. Qi, A. T. Sasaki, D. R. Plas, J. E. Bradner, M. Wei, G. Marcucci, X. Jiang, J. C. Mulloy, J. Jin, C. He, J. Chen, R-2HG exhibits anti-tumor activity by targeting FTO/m^6A/MYC/CEBPA signaling. *Cell* **172**, 90–105.e23 (2018).
14. X. Fu, R. M. Chin, L. Vergnes, H. Hwang, G. Deng, Y. Xing, M. Y. Pai, S. Li, L. Ta, F. Fazlollahi, C. Chen, R. M. Prins, M. A. Teitell, D. A. Nathanson, A. Lai, K. F. Faull, M. Jiang, S. G. Clarke, T. F. Cloughesy, T. G. Graeber, D. Braas, H. R. Christofk, M. E. Jung, K. Reue, J. Huang, 2-Hydroxyglutarate inhibits atp synthase and mTOR signaling. *Cell Metab.* **22**, 508–515 (2015).
15. F. J. Núñez, F. M. Mendez, P. Kadiyala, M. S. Alghamri, M. G. Savelieff, M. B. Garcia-Fabiani, S. Haase, C. Koschmann, A.-A. Calinescu, N. Kamran, M. Saxena, R. Patel, S. Carney, M. Z. Guo, M. Edwards, M. Ljungman, T. Qin, M. A. Sartor, R. Tagett, S. Venneti, J. Brosnan-Cashman, A. Meeker, V. Gorbunova, L. Zhao, D. M. Kremer, L. Zhang, C. A. Lyssiotis, L. Jones, C. J. Hertin, J. L. Ross, D. Hambardzumyan, S. Hervey-Jumper, M. E. Figueroa, P. R. Lowenstein, M. G. Castro, IDH1-R132H acts as a tumor suppressor in glioma via epigenetic up-regulation of the DNA damage response. *Sci. Transl. Med.* **11**, eaaq1427 (2019).
16. P. L. Sulkowski, C. D. Corso, N. D. Robinson, S. E. Scanlon, K. R. Purshouse, H. Bai, Y. Liu, R. K. Sundaram, D. C. Hegan, N. R. Fons, G. A. Breuer, Y. Song, K. Mishra-Gorur, H. M. De Feyter, R. A. de Graaf, Y. V. Surovtseva, M. Kachman, S. Halene, M. Günel, P. M. Glazer, R. S. Bindra, 2-Hydroxyglutarate produced by neomorphic IDH mutations suppresses homologous recombination and induces PARP inhibitor sensitivity. *Sci Transl Med.* **9**, eaal2463 2017).
17. R. J. Molenaar, T. Radivoyevitch, Y. Nagata, M. Khurshed, B. Przychodzen, H. Makishima, M. Xu, F. E. Bleeker, J. W. Wilmink, H. E. Carraway, S. Mukherjee, M. A. Sekeres, C. J. F. van Noorden, J. P. Maciejewski, *IDH1/2* mutations sensitize acute myeloid leukemia to PARP inhibition and this is reversed by IDH1/2-mutant inhibitors. *Clin. Cancer Res.* **24**, 1705–1715 (2018).
18. Y. Lu, J. Kwintkiewicz, Y. Liu, K. Tech, L. N. Frady, Y.-T. Su, W. Bautista, S. I. Moon, J. MacDonald, M. G. Ewend, M. R. Gilbert, C. Z. Yang, J. Wu, Chemosensitivity of

IDH1-mutated gliomas due to an impairment in PARP1-mediated DNA repair. *Cancer Res.* **77**, 1709–1718 (2017).
19. B. Philip, D. X. Yu, M. R. Silvis, C. H. Shin, J. P. Robinson, G. L. Robinson, A. E. Welker, S. N. Angel, S. R. Tripp, J. A. Sonnen, M. W. VanBrocklin, R. J. Gibbons, R. E. Looper, H. Colman, S. L. Holmen, Mutant *IDH1* promotes glioma formation *In Vivo*. *Cell Rep.* **23**, 1553–1564 (2018).
20. H. Wei, X. Yu, Functions of PARylation in DNA damage repair pathways. *Genomics, Proteomics Bioinf.* **14**, 131–139 (2016).
21. J. Murai, S.-Y. N. Huang, B. B. Das, A. Renaud, Y. Zhang, J. H. Doroshow, J. Ji, S. Takeda, Y. Pommier, Trapping of PARP1 and PARP2 by clinical PARP inhibitors. *Cancer Res.* **72**, 5588–5599 (2012).
22. N. J. Curtin, DNA repair dysregulation from cancer driver to therapeutic target. *Nat. Rev. Cancer* **12**, 801–817 (2012).
23. K. A. Reiss, J. M. Herman, D. Armstrong, M. Zahurak, A. Fyles, A. Brade, M. Milosevic, L. A. Dawson, A. Scardina, P. Fischer, A. Hacker-Prietz, R. J. Kinders, L. Wang, A. Chen, S. Temkin, N. Horiba, L.-A. Stayner, L. L. Siu, N. S. Azad, A final report of a phase I study of veliparib (ABT-888) in combination with low-dose fractionated whole abdominal radiation therapy (LDFWAR) in patients with advanced solid malignancies and peritoneal carcinomatosis with a dose escalation in ovarian and fallopian tube cancers. *Gynecol. Oncol.* **144**, 486–490 (2017).
24. Y. Pommier, M. J. O'Connor, J. de Bono, Laying a trap to kill cancer cells: PARP inhibitors and their mechanisms of action. *Sci. Transl. Med.* **8**, 362ps17 (2016).
25. J. Michelena, A. Lezaja, F. Teloni, T. Schmid, R. Imhof, M. Altmeyer, Analysis of PARP inhibitor toxicity by multidimensional fluorescence microscopy reveals mechanisms of sensitivity and resistance. *Nat. Commun.* **9**, 2678 (2018).
26. S. J. Pettitt, D. B. Krastev, I. Brandsma, A. Dréan, F. Song, R. Aleksandrov, M. I. Harrell, M. Menon, R. Brough, J. Campbell, J. Frankum, M. Ranes, H. N. Pemberton, R. Rafiq, K. Fenwick, A. Swain, S. Guettler, J.-M. Lee, E. M. Swisher, S. Stoynov, K. Yusa, A. Ashworth, C. J. Lord, Genome-wide and high-density CRISPR-Cas9 screens identify point mutations in *PARP1* causing PARP inhibitor resistance. *Nat. Commun.* **9**, 1849 (2018).
27. L. M. Wagner, Profile of veliparib and its potential in the treatment of solid tumors. *Onco. Targets Ther.* **8**, 1931–1939 (2015).
28. T. D. Penning, G. D. Zhu, V. B. Gandhi, J. C. Gong, X. S. Liu, Y. Shi, V. Klinghofer, E. F. Johnson, C. K. Donawho, D. J. Frost, V. Bontecheva-Diaz, J. J. Bouska, D. J. Osterling, A. M. Olson, K. C. Marsh, Y. Luo, V. L. Giranda, ABT-888: A potent and orally efficacious inhibitor of poly(ADP-ribose)polymerase. *Abstr. Pap. Am. Chem. S.* **238**, (2009).
29. R. L. Siegel, K. D. Miller, A. Jemal, Cancer statistics, 2019. *CA Cancer J. Clin.* **69**, 7–34 (2019).
30. M. Ghidini, C. Pizzo, A. Botticelli, J. C. Hahne, R. Passalacqua, G. Tomasello, F. Petrelli, Biliary tract cancer: Current challenges and future prospects. *Cancer Manag. Res.* **11**, 379–388 (2019).
31. J. Valle, H. Wasan, D. H. Palmer, D. Cunningham, A. Anthoney, A. Maraveyas, S. Madhusudan, T. Iveson, S. Hughes, S. P. Pereira, M. Roughton, J. Bridgewater; ABC-02 Trial Investigators, Cisplatin plus gemcitabine versus gemcitabine for biliary tract cancer. *N. Engl. J. Med.* **362**, 1273–1281 (2010).
32. E. T. Shinohara, N. Mitra, M. Y. Guo, J. M. Metz, Radiation therapy is associated with improved survival in the adjuvant and definitive treatment of intrahepatic cholangiocarcinoma. *Int. J. Radiat. Oncol. Biol. Phys.* **72**, 1495–1501 (2008).
33. S. Zou, J. Li, H. Zhou, C. Frech, X. Jiang, J. S. C. Chu, X. Zhao, Y. Li, Q. Li, H. Wang, J. Hu, G. Kong, M. Wu, C. Ding, N. Chen, H. Hu, Mutational landscape of intrahepatic cholangiocarcinoma. *Nat. Commun.* **5**, 5696 (2014).
34. D. Hambardzumyan, N. M. Amankulor, K. Y. Helmy, O. J. Becher, E. C. Holland, Modeling adult gliomas using RCAS/t-va technology. *Transl. Oncol.* **2**, 89–IN6 (2009).
35. N. M. Amankulor, Y. Kim, S. Arora, J. Kargl, F. Szulzewsky, M. Hanke, D. H. Margineantu, A. Rao, H. Bolouri, J. Delrow, D. Hockenbery, A. M. Houghton, E. C. Holland, Mutant IDH1 regulates the tumor-associated immune system in gliomas. *Genes Dev.* **31**, 774–786 (2017).
36. Z. Tang, B. Jiang, Z. Shi, W. Gong, Y. Liu, X. Wang, Y. Gao, F. Yu, C. Zhou, L. Luo, M. Wei, L. Wang, Abstract 1651: BGB-290, a novel PARP inhibitor with unique brain penetration ability, demonstrated strong synergism with temozolomide in subcutaneous and intracranial xenograft models. *Cancer Res.* **75**, (2015).
37. Q. T. Ostrom, H. Gittleman, G. Truitt, A. Boscia, C. Kruchko, J. S. Barnholtz-Sloan, CBTRUS statistical report: Primary brain and other central nervous system tumors diagnosed in the united states in 2011-2015. *Neuro. Oncol.* **20**, iv1–iv86 (2018).
38. S. K. Saha, J. D. Gordan, B. P. Kleinstiver, P. Vu, M. S. Najem, J.-C. Yeo, L. Shi, Y. Kato, R. S. Levin, J. T. Webber, L. J. Damon, R. K. Egan, P. Greninger, U. McDermott, M. J. Garnett, R. L. Jenkins, K. M. Rieger-Christ, T. B. Sullivan, A. F. Hezel, A. S. Liss, Y. Mizukami, L. Goyal, C. R. Ferrone, A. X. Zhu, J. K. Joung, K. M. Shokat, C. H. Benes, N. Bardeesy, Isocitrate dehydrogenase mutations confer dasatinib hypersensitivity and SRC dependence in intrahepatic cholangiocarcinoma. *Cancer Discov.* **6**, 727–739 (2016).
39. H. I. Robins, P. Zhang, M. R. Gilbert, A. Chakravarti, J. F. de Groot, S. A. Grimm, F. Wang, F. S. Lieberman, A. Krauze, A. M. Trotti, N. Mohile, A. Y. J. Kee, H. Colman, R. Cavaliere, S. Kesari, S. J. Chmura, M. Mehta, A randomized phase I/II study of ABT-888 in combination with temozolomide in recurrent temozolomide resistant glioblastoma: An NRG oncology RTOG group study. *J. Neurooncol* **126**, 309–316 (2016).
40. E. Shaw, R. Arusell, B. Scheithauer, J. O'Fallon, B. O'Neill, R. Dinapoli, D. Nelson, J. Earle, C. Jones, T. Cascino, D. Nichols, R. Ivnik, R. Hellman, W. Curran, R. Abrams, Prospective randomized trial of low- versus high-dose radiation therapy in adults with supratentorial low-grade glioma: Initial report of a north central cancer treatment group/radiation therapy oncology group/eastern cooperative oncology group study. *J. Clin. Oncol.* **20**, 2267–2276 (2002).
41. L. A. Dawson, C. J. McGinn, D. Normolle, R. K. Ten Haken, S. Walker, W. Ensminger, T. S. Lawrence, Escalated focal liver radiation and concurrent hepatic artery fluorodeoxyuridine for unresectable intrahepatic malignancies. *J. Clin. Oncol.* **18**, 2210–2218 (2000).
42. C. H. Crane, K. O. Macdonald, J. N. Vauthey, P. Yehuda, T. Brown, S. Curley, A. Wong, M. Delclos, C. Charnsangavej, N. A. Janjan, Limitations of conventional doses of chemoradiation for unresectable biliary cancer. *Int. J. Radiat. Oncol. Biol. Phys.* **53**, 969–974 (2002).
43. S. Turcan, A. W. M. Fabius, A. Borodovsky, A. Pedraza, C. Brennan, J. Huse, A. Viale, G. J. Riggins, T. A. Chan, Efficient induction of differentiation and growth inhibition in IDH1 mutant glioma cells by the DNMT Inhibitor Decitabine. *Oncotarget* **4**, 1729–1736 (2013).
44. M. S. Waitkus, C. J. Pirozzi, C. J. Moure, B. H. Diplas, L. J. Hansen, A. B. Carpenter, R. Yang, Z. Wang, B. O. Ingram, E. D. Karoly, R. P. Mohney, I. Spasojevic, R. E. McLendon, H. S. Friedman, Y. He, D. D. Bigner, H. Yan, Adaptive evolution of the GDH2 allosteric domain promotes gliomagenesis by resolving IDH1^{R132H}-induced metabolic liabilities. *Cancer Res.* **78**, 36–50 (2018).
45. J. Silber, A. Jacobsen, T. Ozawa, G. Harinath, A. Pedraza, C. Sander, E. C. Holland, J. T. Huse, miR-34a repression in proneural malignant gliomas upregulates expression of its target PDGFRA and promotes tumorigenesis. *PLOS ONE* **7**, e33844 (2012).
46. B. M. Gyori, G. Venkatachalam, P. S. Thiagarajan, D. Hsu, M.-V. Clement, OpenComet: An automated tool for comet assay image analysis. *Redox Biol.* **2**, 457–465 (2014).
47. E. Tchougounova, M. Kastemar, D. Bråsäter, E. C. Holland, B. Westermark, L. Uhrbom, Loss of Arf causes tumor progression of PDGFB-induced oligodendroglioma. *Oncogene* **26**, 6289–6296 (2007).

Acknowledgments: We thank the Chan lab for discussions. We thank C. Thompson for advice. **Funding:** This work was supported in part by the U.S. NIH (R01 CA177828) (to T.A.C.) and NIH Core Grant P30 CA008748. **Author contributions:** The study was designed by T.A.C., Y.W., and A.T.W. Experiments were performed by Y.W., A.T.W., S.T., W.H.W., X.M., and Y.G. Results were interpreted by T.A.C., Y.W., A.T.W., and J.T.H. Pathologic samples were provided and characterized by D.S.K. and C.S. T.A.C., Y.W., and A.T.W. wrote the paper with input from all authors. **Competing interests:** T.A.C. is an inventor on provisional patent application (62/569,053) submitted by MSKCC that covers use of tumor mutational burden as a predictive biomarker for cancer immunotherapy. T.A.C. is an inventor on patent application (PCT/US2015/062208) filed by MSKCC, relating to the use of TMB in lung cancer immunotherapy that has been licensed to Personal Genome Diagnostics, and MSKCC and T.A.C. receive royalties. T.A.C. is a cofounder of Gritstone Oncology and holds equity in An2H. T.A.C. has served as an advisor for Bristol-Myers Squibb, Illumina, Eisai, and An2H. The other authors declare that they have no competing interests. **Data and materials availability:** All data needed to evaluate the conclusions in the paper are present in the paper and/or the Supplementary Materials. Additional data related to this paper may be requested from the authors.

Submitted 29 August 2019
Accepted 21 January 2020
Published 22 April 2020
10.1126/sciadv.aaz3221

Citation: Y. Wang, A. T. Wild, S. Turcan, W. H. Wu, C. Sigel, D. S. Klimstra, X. Ma, Y. Gong, E. C. Holland, J. T. Huse, T. A. Chan, Targeting therapeutic vulnerabilities with PARP inhibition and radiation in IDH-mutant gliomas and cholangiocarcinomas. *Sci. Adv.* **6**, eaaz3221 (2020).